Supplementary Information

Interplay of Charge Density Wave Transition with Topological and Superconducting Properties

Zishen Wang,[1,2] Jing-Yang You, [1] Chuan Chen,[3,4] Jinchao Mo,[1] Jingyu He,[1] Lishu

Zhang,[1] Jun Zhou,[5,*] Kian Ping Loh,[2,6,*] Yuan Ping Feng[1,2,*]

[1] Department of Physics, National University of Singapore, 117542 Singapore, Singapore

[2] Centre for Advanced 2D Materials, National University of Singapore, 117546 Singapore, Singapore

[3] Institute for Advanced Study, Tsinghua University, 100084 Beijing, China

[4] Max-Planck Institute for the Physics of Complex Systems, 01187 Dresden, Germany

[5] Institute of Materials Research & Engineering, A*STAR (Agency for Science, Technology, and Research), 138634 Singapore, Singapore.

[6] Department of Chemistry, National University of Singapore, 117543 Singapore, Singapore

* Corresponding authors:

Jun Zhou (zhou_jun@imre.a-star.edu.sg)

Kian Ping Loh (chmlohkp@nus.edu.sg)

Yuan Ping Feng (phyfyp@nus.edu.sg)

I. Spectral Function in a One-band Mean-field Model

We consider a 2D, one-band model with the mean-field Hamiltonian:

$$H_k = \sum_k \varepsilon_k c_k^\dagger c_k + \sum_{k,i} 2\Delta g_{k,k+Q_i} c_k^\dagger c_{k+Q_i} + h.c., \#(S1)$$

where $c_k^\dagger$ and c_k are electron operators, ε_k is the energy. $g_{k,k+Q_i}$ is the EPC matrix element. Δ is the order parameter that is approximated to be a constant due to the small pocket size and rotation symmetry.
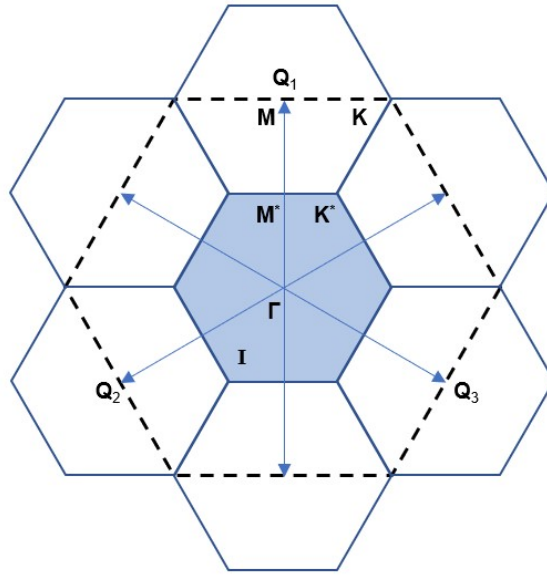

Figure S1. Black dashed hexagon: first Brillouin zone of normal phase. Blue shaded region I: first BZ of 2×2 CDW phase. Q_i (i = 1-3) are CDW vectors.

Here we use 2×2 CDW as an example. As shown in Figure S1, the reduced BZ of this CDW phase is 4 times smaller than the normal one. Each **k** point in the reduced BZ will connect other **k** points in the other 3 small hexagons by the EPC matrix element $g_{k,k+Q_i}$. Therefore, the mean-field Hamiltonian can be modified as:

$$H_k = \sum_{k \in I} \left[c_k^\dagger \ c_{k+Q_1}^\dagger \ c_{k+Q_2}^\dagger \ c_{k+Q_3}^\dagger \right] h_k \begin{bmatrix} c_k \\ c_{k+Q_1} \\ c_{k+Q_2} \\ c_{k+Q_2} \end{bmatrix}, \#(S2)$$

with

$$h_k = \begin{bmatrix} \varepsilon_k & 2\Delta g_{k,k+Q_1} & 2\Delta g_{k,k+Q_2} & 2\Delta g_{k,k+Q_3} \\ 2\Delta g_{k+Q_1,k} & \varepsilon_{k+Q_1} & 2\Delta g_{k+Q_1,k+Q_2} & 2\Delta g_{k+Q_1,k+Q_3} \\ 2\Delta g_{k+Q_2,k} & 2\Delta g_{k+Q_2,k+Q_1} & \varepsilon_{k+Q_2} & 2\Delta g_{k+Q_2,k+Q_3} \\ 2\Delta g_{k+Q_3,k} & 2\Delta g_{k+Q_3,k+Q_1} & 2\Delta g_{k+Q_3,k+Q_2} & \varepsilon_{k+Q_3} \end{bmatrix}. \#(S3)$$

Then we have the retarded electronic Green function:

$$G_{k,\omega} = \frac{1}{\omega - H_k + i\delta}. \#(S4)$$

The spectral function can be calculated as:

$$A_{k,\omega} = \frac{1}{\pi} Im G_{k,\omega} \#(S5)$$

The spectral function of the 3×3 CDW structure can be derived in the same way.

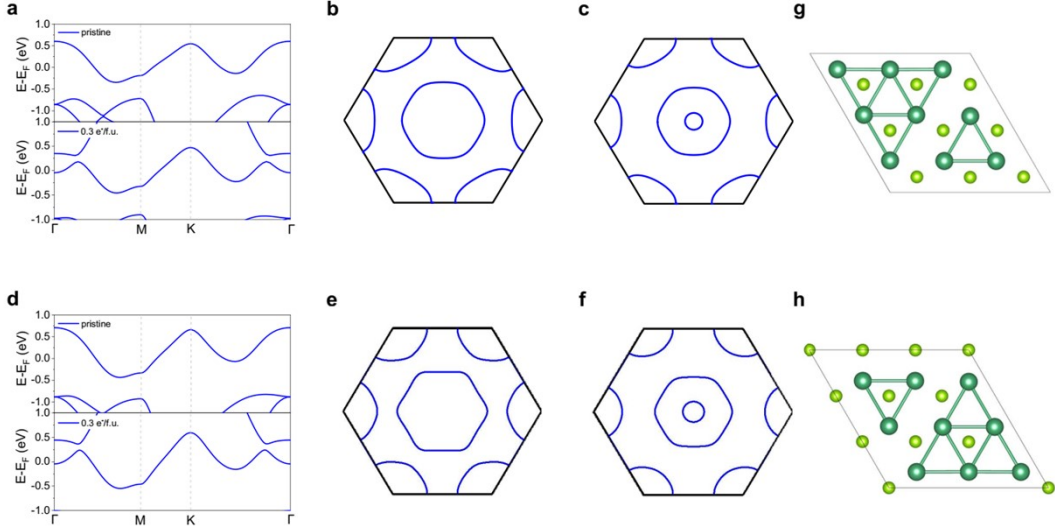## II. General Properties of Monolayer 1H-MSe$_2$

Figure S2. (a) Band structure of normal phase of NbSe$_2$ without doping (up panel) and with 0.3 e$^-$/f.u. doping concentration (down panel). Fermi surfaces of NbSe$_2$ (b) without doping and (c) with 0.3 e$^-$/f.u. doping concentration. (d-f) Same as panels (a-c) but for TaSe$_2$. (g) 3×3 hollow and (h) 3×3 filled CDW structures.

Figure S2a is the band structures of monolayer 1H-NbSe$_2$ with and without doping, in which both have one band crosse the Fermi level, forming the Fermi surface as shown in Figures S2b and S2c. Such an electronic band is considered in the calculation of EPC matrix elements. Figure S2d is the band structures of monolayer 1H-TaSe$_2$ with and without doping, which display similar Fermi surface patterns as in 1H-NbSe$_2$ (Figures S2e and S2f). It is noted that the bands near the Γ point are largely modulated by electron doping, which forms an additional electron pocket at the Γ point (Figures S2c and S2f). Figures S2g and S2h are two possible CDW structures of pristine 1H-MSe$_2$ (M = Nb, Ta). The 3×3 hollow CDWs are the ground states as their energies are a bit lower than the 3×3 filled CDW (Figure 1e).
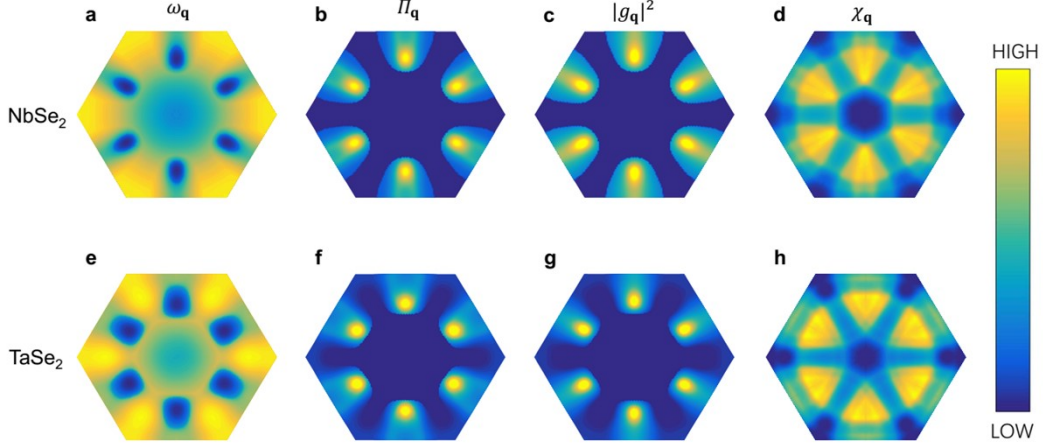
III. CDW Formation in Pristine 1H-MSe$_2$.

Figure S3. (a) The softened phonon frequency ω_q, (b) the real part of the phonon self-energy Π_q, (c) **q**-EPC $|g_q|^2$ and (d) the real part of the bare electronic susceptibility χ_q in the first BZ of pristine NbSe$_2$. (e-h) Same as panels (a-d) but for pristine TaSe$_2$.

Figure S3a indicates that the imaginary phonons of NbSe$_2$ are concentrated in the egg shape centered at 2/3 ΓM. Meanwhile, a complementary pattern can be found for the real part of the phonon self-energy Π_q, which displays a peak at 2/3 ΓM, in line with the dip in ω_q. In addition, the topology of $|g_q|^2$ is very close to Π_q. However, the χ_q shows the plateau in a fan-shaped region around 2/5 ΓM (see the yellow region in Figure S3d), which deviates from the dip of ω_q in Figure S3a and the peak of Π_q in Figure S3b. For pristine TaSe$_2$, the $|g_q|^2$ and Π_q also have similar patterns, corresponding to the distribution of ω_q. The χ_q still cannot match the phonon softening in Figure S3e. Therefore, we conclude that the **q**-EPC accounts for the 3×3 CDW formation in both NbSe$_2$ and TaSe$_2$.
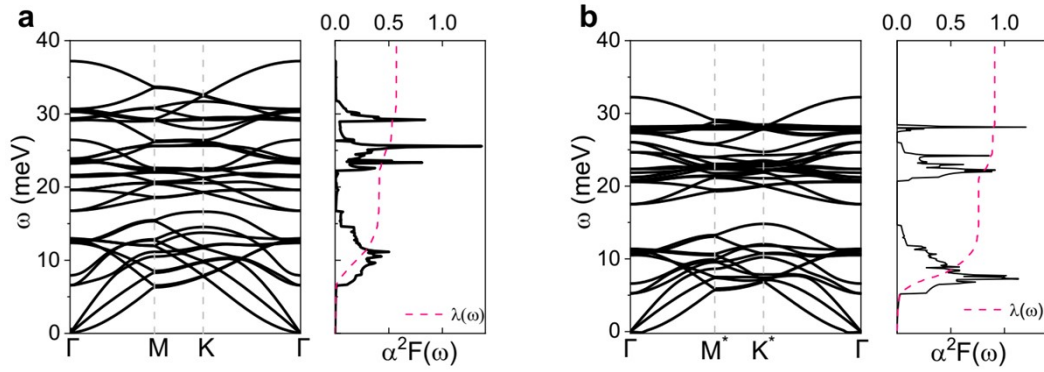
IV. Superconductivity in 2×2 Hollow CDWs.

Figure S4. The Phonon spectra, Eliashberg spectral functions $\alpha^2 F(\omega)$ and frequency-dependent integrated EPC $\lambda(\omega)$ of 2×2 hollow CDWs under 0.3 e⁻/f.u. doping concentration for (a) NbSe$_2$ and (b) TaSe$_2$.

The 2×2 hollow CDWs not only have nontrivial topology, but also have superconductivity. Figure S4 reveals that the hollow CDWs have larger total EPC strength $\lambda =$ 0.57 and 0.91, which induce enhanced $T_c =$ 1.2 K and 4.4 K for NbSe$_2$ and TaSe$_2$, respectively.